Influence of the Eurasian snow cover on the Indian summer monsoon variability in observed climatologies and CMIP3 simulations

Y. Peings · H. Douville

Abstract The present study is aimed at revisiting the possible influence of the winter/spring Eurasian snow cover on the subsequent Indian summer precipitation using several statistical tools including a maximum covariance analysis. The snow–monsoon relationship is explored using both satellite observations of snow cover and in situ measurements of snow depth, but also a subset of global coupled ocean–atmosphere simulations from the phase 3 of the Coupled Model Intercomparison Project (CMIP3) database. In keeping with former studies, the observations suggest a link between an east–west snow dipole over Eurasia and the Indian summer monsoon precipitation. However, our results indicate that this relationship is neither statistically significant nor stationary over the last 40 years. Moreover, the strongest signal appears over eastern Eurasia and is not consistent with the Blanford hypothesis whereby more snow should lead to a weaker monsoon. The twentieth century CMIP3 simulations provide longer timeseries to look for robust snow–monsoon relationships. The maximum covariance analysis indicates that some models do show an apparent influence of the Eurasian snow cover on the Indian summer monsoon precipitation, but the patterns are not the same as in the observations. Moreover, the apparent snow–monsoon relationship generally denotes a too strong El Niño-Southern Oscillation teleconnection with both winter snow cover and summer monsoon rainfall rather than a direct influence of the Eurasian snow cover on the Indian monsoon.

1 Introduction

The understanding and long-range forecasting of the Indian summer monsoon is an important and difficult challenge for the climate research community. This phenomenon has a strong impact on the food production, the water resources and the whole economy of one of the most populated areas in the world. Therefore, obtaining an accurate prediction of monsoon rainfall has been an important research topic since several decades. The role of the El Niño Southern Oscillation (ENSO) on the interannual fluctuations of the Indian monsoon has been extensively documented (Walker 1924; Rasmusson and Carpenter 1983; Shukla and Paolino 1983) and is widely admitted by the climate community. Another potential source of seasonal persistence in the Asian region is the continental snow cover because of its strong influence on the land surface energy budget and thereby on the land-sea temperature contrast that is presumably driving the monsoon circulation.

In particular, the possible influence of the Eurasian winter/spring snow cover on the Indian summer monsoon rainfall is an old debate. The first study on the subject dates back 1884, when Sir William T. Blanford found an inverse relationship between Himalayan winter/spring snow accumulation and the amount of precipitation over India during the subsequent summer (Blanford 1884). He identified a local influence involving dry winds sweeping down from

Y. Peings · H. Douville
CNRM-GAME, MétéoFrance-CNRS, Toulouse, France

Y. Peings (✉)
CNRM/GMGEC/UDC, 42 avenue Gaspard Coriolis, 31057
Toulouse Cedex 01, France
e-mail: yannick.peings@cnrm.meteo.fr

the mountains following each precipitation event that would evaporate the fallen rain in plains and in return would reduce the subsequent local source of moisture for precipitation. He also pointed out that remote large scale atmospheric anomalies could exert an influence on pressure pattern over India and thus over the monsoon onset. Walker (1910) followed up his study and confirmed the inverse relationship between the two parameters.

Using the satellite observations of snow cover provided by the National Oceanic and Atmospheric Administration (NOAA) since 1967, studies re-examined the subject during the 1980s and 1990s (Hahn and Shukla 1976; Dey and Bhanu Kumar 1982; Dickson 1984; Ropelewski et al. 1984; Dey et al. 1985; Yang 1996; Parthasarathy and Yang 1995; Sankar-Rao et al. 1996; Matsuyama and Masuda 1998; Bamzai and Shukla 1999). All these studies concluded that a positive (negative) anomaly of snow cover over Eurasia or some part of Eurasia during winter or spring is followed by an anomalous weak (strong) monsoon during subsequent summer. However, Bamzai and Shukla (1999) found that the only region for which a significant inverse correlation exists between winter snow cover and subsequent summer monsoon rainfall is western Eurasia. In contrast to the Blanford hypothesis, no significant correlation was found between the Himalayan snow cover and subsequent monsoon rainfall. Some authors achieved similar studies using snow depth rather than snow cover data, notably the station data of former USSR and the Scanning Multifrequency Microwave Radiometer (SMMR) satellite data (Kripalani and Kulkarni 1999; Ye and Bao 2001; Dash et al. 2004). One of their principal conclusions was that the snow pattern associated with the Indian monsoon rainfall is not homogeneously distributed but is more resembling a dipole-type structure with opposite sign anomalies over western and eastern Eurasia.

Several modelling studies have been more or less successful to capture the observed snow–monsoon relationship and have suggested some possible physical mechanisms for the winter to summer climate memory (Barnett et al. 1989; Yasunari et al. 1991; Vernekar et al. 1995; Douville and Royer 1996; Ferranti and Molteni 1999). In summary, heavy snowfall during winter perturbs the land surface energy budget from spring to early summer, a significant part of the solar radiation being used first to melt the snowpack, then to evaporate the resulting soil moisture. This leads to lower land surface temperature, i.e. a reduction of the thermal contrast between the Eurasian continent and the Indian Ocean, and thereby a weakening of summer monsoon circulation.

Recently, this snow–monsoon linkage was questioned by Shinoda (2001) and Robock et al. (2003), who found that there was no evidence for a large scale land surface memory effect that could influence the Indian monsoon through soil moisture. Fasullo (2004) attempted to reconcile these results with the previous modelling studies by exploring the snow–monsoon link as a part of the ENSO-monsoon connection, and suggested that the influence of land surface could be overwhelmed by the ENSO variability but identified for neutral ENSO years.

The present study is first aimed at revisiting this topic using both in situ and satellite observations, the latter being now available over a 40-year period that allows us to evaluate the robustness and stability of the snow–monsoon relationship. The second objective is to look for such a relationship in the historical coupled ocean-atmosphere simulations of the Coupled Model Intercomparison Project 3 (CMIP3) database. The main idea here is to investigate whether or not state-of-the-art global climate models are likely to simulate the interannual variability of the Eurasian snow cover and its possible influence on the Indian summer monsoon rainfall over a period that encompasses the whole twentieth century.

2 Data and methods

2.1 Observations

To describe the Indian summer monsoon precipitation, we use the All-India-Rainfall (AIR) index estimated from June to September (JJAS) which is available over the 1871–2005 period. This index is an area weighted average from 29 Indian Rainfall subdivisions (Parthasarathy et al. 1995). We also use the Climate Research Unit CRU2 precipitation climatology, which is provided at the 0.5° resolution for the 1901–2002 period and based only on rain-gauge measurements, and the CRU2 2 m-temperature climatology for the 1901–2002 period based on station data. These datasets have been here interpolated onto a 128 by 64 horizontal grid (2.8° resolution) to be close to the medium resolution of the CMIP3 models.

The monthly snow cover climatology is derived from the Northern Hemisphere weekly snow cover extent Version 3 product (Armstrong and Brodzik 2005), available at the National Snow and Ice Data Center (NSIDC). This dataset extends from 3 October 1966 through 24 June 2007 and has been also interpolated on a 128 by 64 horizontal grid. Each grid cell contains one bit of information for each week indicating the absence or presence of snow cover and is reported on a 25 km Equal-Area Scalable Earth Grid (EASE-Grid) that spans the whole Northern Hemisphere. Snow cover extent is based on the digital NOAA National Environmental Satellite, Data and Information Service (NESDIS) weekly snow charts, revised and interpolated on the EASE grid. Since 1997, NOAA snow maps are constructed digitally by the Interactive Multisensor Snow and

Ice Mapping System (Helfrich et al. 2007). Prior to this, they were based on a visual interpretation of photographic copies of shortwave imagery by trained meteorologists. Up to 1972, the resolution of the meteorological satellites commonly used was around 4 km. Beginning in October 1972, the Very High Resolution Radiometer (VHRR) provided imagery with a spatial resolution of 1.0 km, which in November 1978, with the launching of the Advanced VHRR (AVHRR), was reduced slightly to 1.1 km. The monthly fraction of snow cover on each pixel has been obtained by averaging weekly data. Some gaps exist in the dataset during July 1968, June–October 1969, and July–September 1971, but they do not affect our analysis because of our interest in the winter and spring season only. It was therefore decided to also use these years in our study.

The monthly mean snow depth data over Eurasia have been obtained from the Historical Soviet Daily Snow Depth Version II (HSDSD-II) data set of NSIDC (Armstrong 2001). This dataset from the former Soviet Union provides long-term daily snow depths for 1881 to 1995 and updates the original HSDSD-I dataset also available from NSIDC. The HSDSD data were extracted from the Soviet meteorological archive, which contains daily data from World Meteorological Organization (WMO) stations over this region. HSDSD includes daily snow depth which is used in this study to compute the monthly mean snow depth for all the 284 WMO stations. The geographical distribution of the stations is between 35°N and 72°N and between 20°E and 180°E. This dataset has been updated from 1881 through 1995 using an improved data quality control. We have considered only the period 1936–1995 because the number of stations varied in time, and most of the data were observed between 1936 and 1995 (Kripalani and Kulkarni 1999). The dataset has been interpolated onto a $1 \times 1°$ resolution grid, with missing values in pixels without station data. Other pixels represent one station data or the average between two stations data.

Finally, a winter index of the North Atlantic Oscillation (NAO) over the whole twentieth century (Hurrell et al. 2003) was defined using the normalized sea-level pressure difference averaged from December to February between Lisbon and Stykkisholmur, calculated with the HadSLP2 dataset provided by the Hadley Centre of the UK Met Office (1850–2003, available at http://hadobs.metoffice.com/index.html). The Met Office Hadley Centre's sea surface temperature (SST) data set HadSST2 have been used to create an ENSO index after interpolation onto the 128×64 horizontal grid.

2.2 Models

The global coupled ocean-atmosphere simulations that have been explored in the present study belong to the World Climate Research Programme's (WCRP's) CMIP3 multi-model dataset. A subset of nine among the 25 CMIP3 models has been selected, which includes most models involved in the ENSEMBLES European project as well as the NCAR and MRI models (Table 1). A relatively detailed model documentation can be found at http://www-pcmdi.llnl.gov/ipcc/model_documentation/ipcc_model_documentation.php. The present study only makes use of the historical simulations, i.e. integrations from the mid-nineteenth century to the end of the tewntieth century driven by observed concentrations of greenhouse gases and, at least, sulfate aerosols (20C3M simulations). A single realization is analysed for each model. A global evaluation of the simulations can be found in chapter 8 of the Intergovernmental Panel on Climate Change 4th Assessment report (IPCC-AR4). While the selected subset of models is not aimed at providing a comprehensive description of the models behaviour, it encompasses a relatively wide range of model resolutions, dynamical cores and physical packages and is hopefully representative of the variety of snow–monsoon relationships simulated in coupled ocean–atmosphere General Circulation Models (GCMs). Note finally that the monthly outputs of all models have been analysed on their original grid.

2.3 Statistical tools
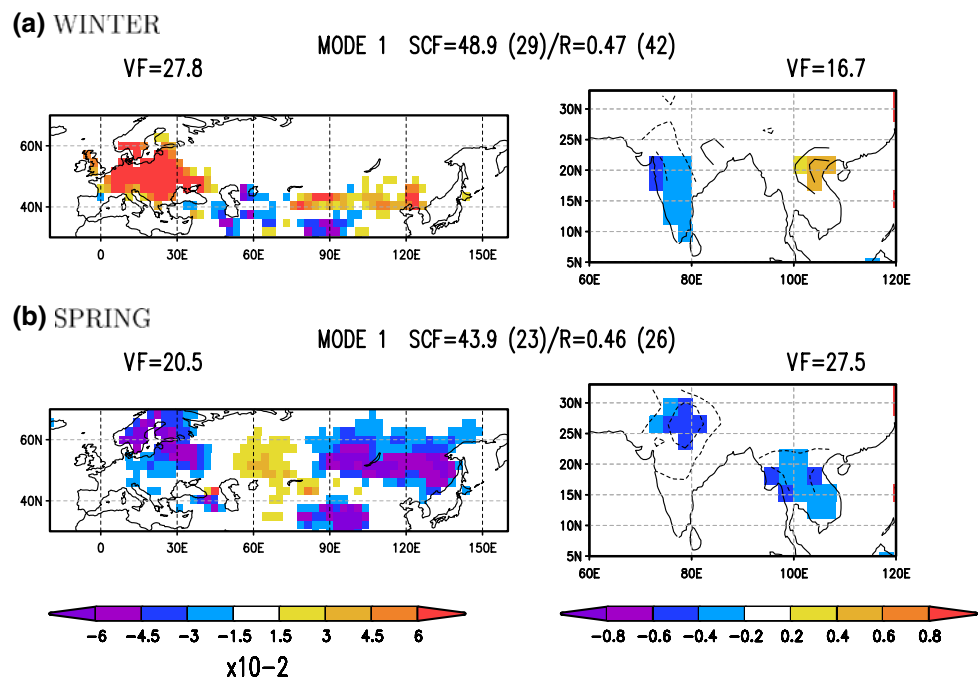
They can be summarized as follows:

- Possible trends in the timeseries have been removed using a simple linear fit for observations. For model outputs, the timeseries are the concatenation of the twentieth and twenty-first centuries, thereby allowing us to use a 3rd order polynomial that is more consistent with the prescribed radiative forcing and with the simulated global warming.
- A phase-scramble bootstrap test is used to determine the statistical significance of the correlations which takes into account the possible auto-correlation in the timeseries. The bootstrap procedure is applied 9999 times to

Table 1 Acronym given to the 20C3M simulations selected from the IPCC-AR4 CMIP3 database

Acronym	Model ID, country
BCCR	BCCR-BCM2.0, Norway
CNRM	CNRM-CM3, France
HADCM3	UKMO-HadCM3, UK
HADGEM1	UKMO-HadGEM1, UK
IPSL	IPSL-CM4, France
MPI	ECHAM5/MPI-OM, Germany
MRI	MRI-CGCM2.3.2, Japan
NCAR	CCSM3, USA

Corresponding model identifier and country of the laboratory

Fig. 1 Maximum covariance analysis between: (**a**) DJF, (**b**) MAM snow cover fraction (*left*) and subsequent JJAS precipitation in mm/day (right) over the 1967–2002 period. First homogeneous vector are shown for snow cover and first heterogeneous vector for precipitation. The fraction of explained covariance (SCF) and the correlation between the two expansion coefficients are indicated, with the confidence level in parentheses

suppress the chronology in the timeseries and a correlation is recalculated at each step. A confidence level of 99% means that 99% of the "random" correlations are less than the original correlation.

- The principal component analysis (PCA) has been used to define seasonal ENSO indices from the simulated SST.
- Composites analysis have been used to characterize the snow cover departures for strongly positive and negative monsoon years, which have been defined as the years having an AIR index exceeding one standard deviation. Similarly, strong and weak NAO years have respectively a normalized index above 1 or below −1. The significance of the composite anomalies has been assessed with the method described in Terray et al. (2003), as advised by Nicholls (2001).
- Also called singular vector decomposition, the maximum covariance analysis (MCA), has been used to relate snow and precipitation patterns (Bretherton et al. 1992). It can be considered as a generalization of the PCA, and indeed reduces to it when the two fields are identical. It is aimed at computing the covariance matrix between two fields and at defining some pairs of spatial patterns which describe a fraction of the total square covariance (SCF). The SCF is a measure of the relative importance of each mode in the relationship between two fields. The expansion coefficient (EC) for each variable is computed by projecting the respective data field onto the corresponding singular vector. The correlation value (R) between the EC of the two variables indicates how strongly related the coupled patterns are.

Using the EC timeseries from the MCA, two types of maps can be generated:

- The kth homogeneous vector is the regression map between the grid point anomalies of a given field and its kth EC. It provides the pattern of the co-varying part between the field and the kth EC.
- The kth heterogeneous vector is the regression map between the grid point anomalies of a given field and the kth EC of the other field. It indicates how well the grid point anomalies of one field can be predicted from the knowledge of the kth EC of the other field.

Significance levels for SCF and R are estimated using a moving block bootstrap procedure as described in Wilks (1997). Each MCA is repeated 99 times, linking one of the field anomaly with the randomly scrambled other, so that the chronological order between the two fields is destroyed. The possible influence of serial correlation is reduced by considering blocks of two successive years in the shuffling of the time sequence. Significance levels for SCF (respectively R) are estimated by the percentage of randomized SCF (respectively R) for the corresponding mode that exceeds the value being tested. By example, for a given mode, a confidence level reaching 95 for SCF (R) means that 95 among the 99 "random" MCA exceed the value of SCF (R). Concerning heterogeneous maps, significance levels are computed at each grid point using an ordinary permutation test with 99 shuffles (Von Storch and Zwiers 1999), and colour shades indicates the heterogeneous vector in each grid point where the correlation is significant at the 95% level. The first step in MCA involves

Fig. 2 Anomalies and 11-years sliding correlations between Eurasian snow cover [30–80N/20W–140E] and the AIR index for the period 1967–2005: **a** and **b** for winter snow cover, **c** and **d** for spring snow cover. *Horizontal dashed lines* represent the 95% confidence level
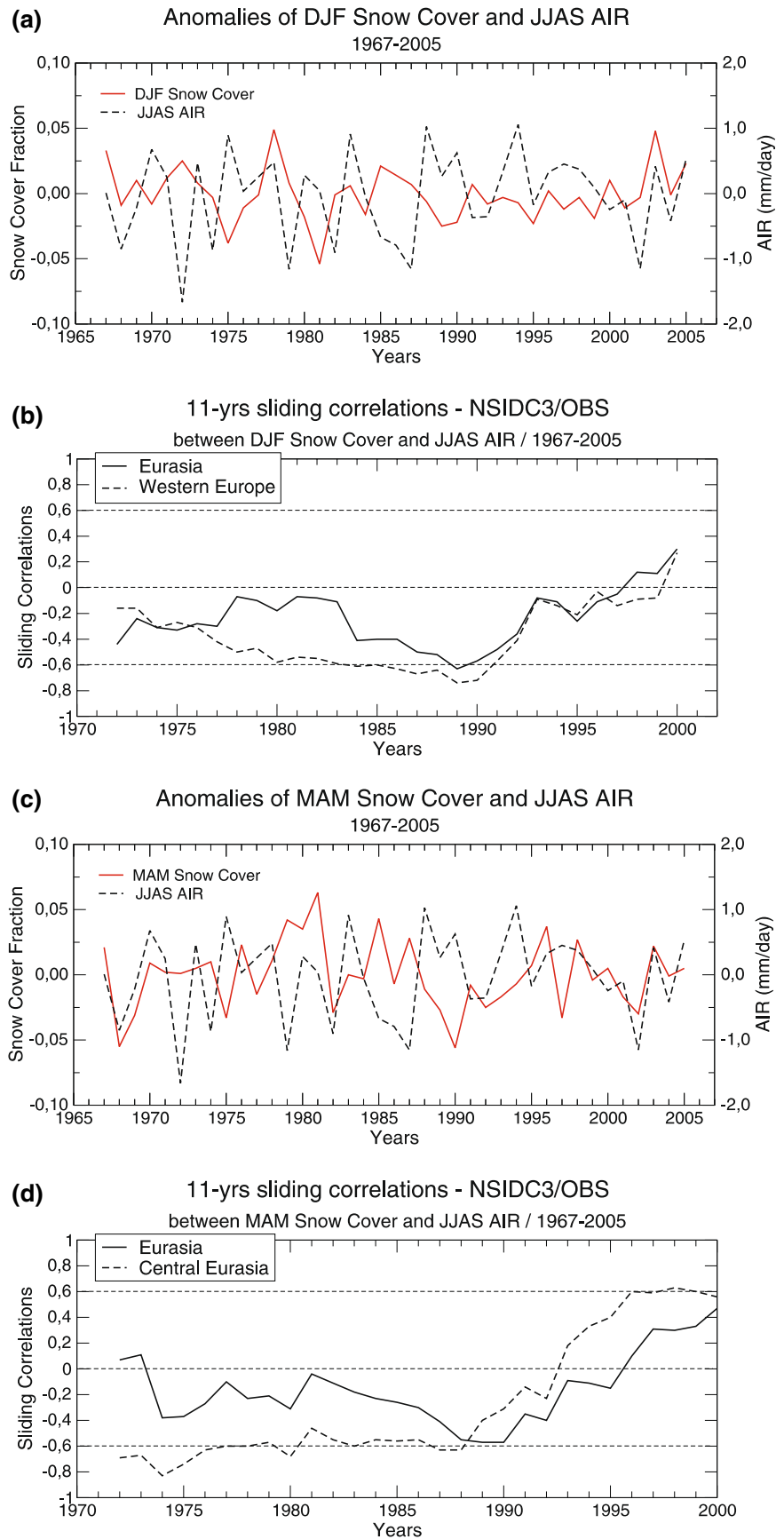

(a) Anomalies of DJF Snow Cover and JJAS AIR
1967-2005

(b) 11-yrs sliding correlations - NSIDC3/OBS
between DJF Snow Cover and JJAS AIR / 1967-2005

(c) Anomalies of MAM Snow Cover and JJAS AIR
1967-2005

(d) 11-yrs sliding correlations - NSIDC3/OBS
between MAM Snow Cover and JJAS AIR / 1967-2005

Table 2 Correlation coefficients between DJF and MAM seasonal snow cover anomalies over entire Eurasia, western Eurasia and northwest Eurasia and JJAS AIR for the period 1967–2005

Domain	Winter (DJF)	Spring (MAM)
Eurasia [30–80N/20W–140E]	−0.17	−0.06
Western Europe [35–60N/10W–30E]	***−0.35***	−0.03
Central Eurasia [40–65N/45–75E]	0.09	−0.28

Values exceeding the 90%, 95% and 99% confidence levels are shown in italic, bold, bold and italic, respectively

a filtering of the anomaly fields to limit the amount of noise present in the data. An empirical orthogonal function (EOF) decomposition of each input field is computed and fields are reconstructed by summing the projection of the raw anomalies on the principal components of the first modes of EOF. The number of modes is determined so as to keep at least 60% of the total variance for each field. This criterion allows us to remove the modes which represent less than 5% of the total variance in the field and thereby to reduce the amount of noise by eliminating poorly organized small-scales features of the snow and precipitation fields.

3 Snow–monsoon relationship in satellite and in situ observations

3.1 Results of the MCA

To explore the possible relationship between the Eurasian snow cover and the Indian summer (JJAS for June–July–August–September mean) monsoon rainfall, we performed two maximum covariance analysis between snow cover

over Eurasia and summer precipitation over India for the period 1967–2002. We distinguish between the winter and spring seasonal anomalies of snow cover (Fig. 1). Filtering of each field has been achieved prior to the MCA calculation (see Sect. 2.3 for details). Our goal is to characterize the leading pattern of snow cover which could influence the subsequent monsoon precipitation over India. For this reason, we show homogeneous vectors for snow cover and heterogeneous vectors for precipitation. Only the first modes of MCA are presented, which capture 48.9 and 43.9% of the total covariance between the two fields for winter and spring, respectively. Without prior spatial filtering, these percentages are much smaller, with respectively 18 and 20% of SCF explained. Weak monsoon precipitation over western India is associated with a strong snow cover over Europe in winter. In agreement with the results of Bamzai and Shukla (1999), there is no clear signal over the rest of the Eurasian continent. Note also that SCF and R are not significant at the 90% confidence level. In spring, the first mode shows that a weak monsoon over northern rather than western India is preceded by a tripole-like pattern of anomalous snow cover, with an excess of snow over central Eurasia but a deficit over the western and eastern parts of the continent. A direct relationship is also found between the Himalayan snow cover and northern Indian monsoon rainfall in agreement with previous studies. Here again, SCF and R are however not significant at the 90% confidence level. Note that the same results are obtained when June-July mean and August-September mean are considered for the AIR index.

In summary, these first results are in qualitative agreement with previous studies (Bamzai and Shukla 1999; Robock et al. 2003; Fasullo 2004) about the pattern of seasonal snow cover anomalies associated with the monsoon rainfall variability. Nevertheless, they indicate that

Fig. 3 Scatterplot between snow cover fraction over Eurasia and JJAS AIR for the period 1967–2005: **a** for winter snow cover; **b** for spring snow cover. Based on preceding DJF SST Niño3.4, the El Niño years are shown as *red squares*, the La Niña years are shown as *green triangles*. Others are shown as *black circles*. The regression line slopes are also plotted for years without DJF ENSO events
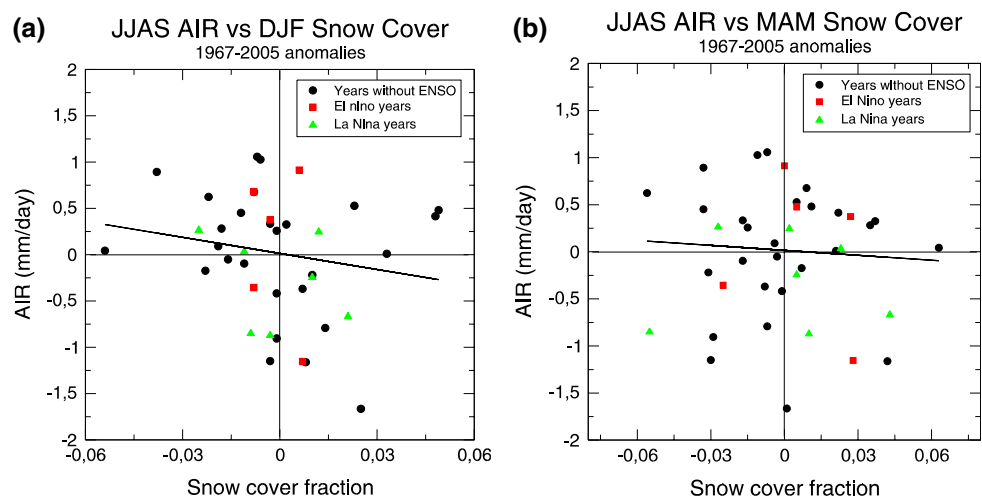
Fig. 4 Composites of snow cover fraction for strong minus weak monsoons for the period 1967–2005: **a** winter snow cover **b** spring snow cover **c** spring snow cover, years with strong winter NAO index removed. *Stippled areas* represents the 90% confidence level. Number of years selected for the computation of the composites + and − are annotated
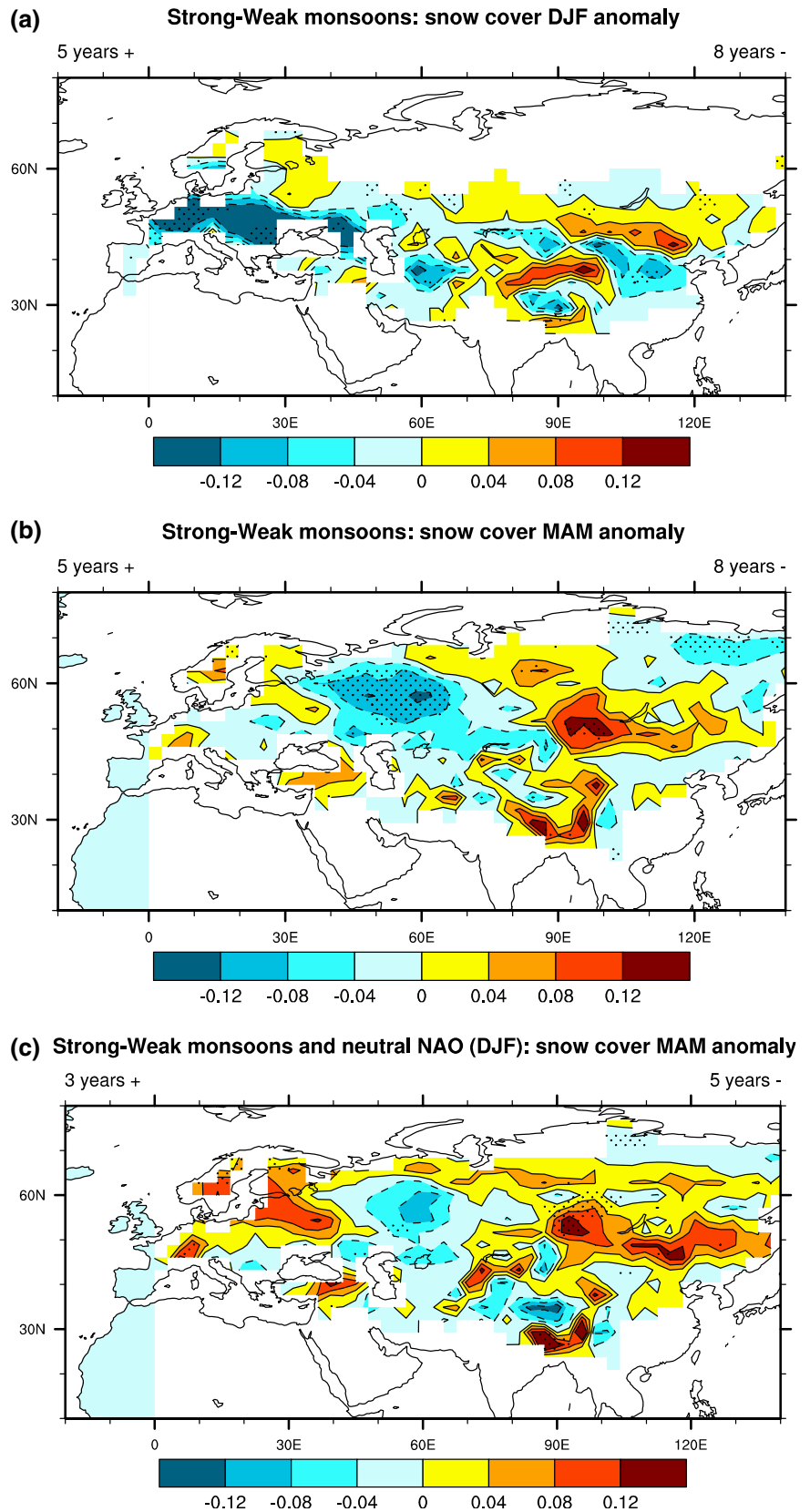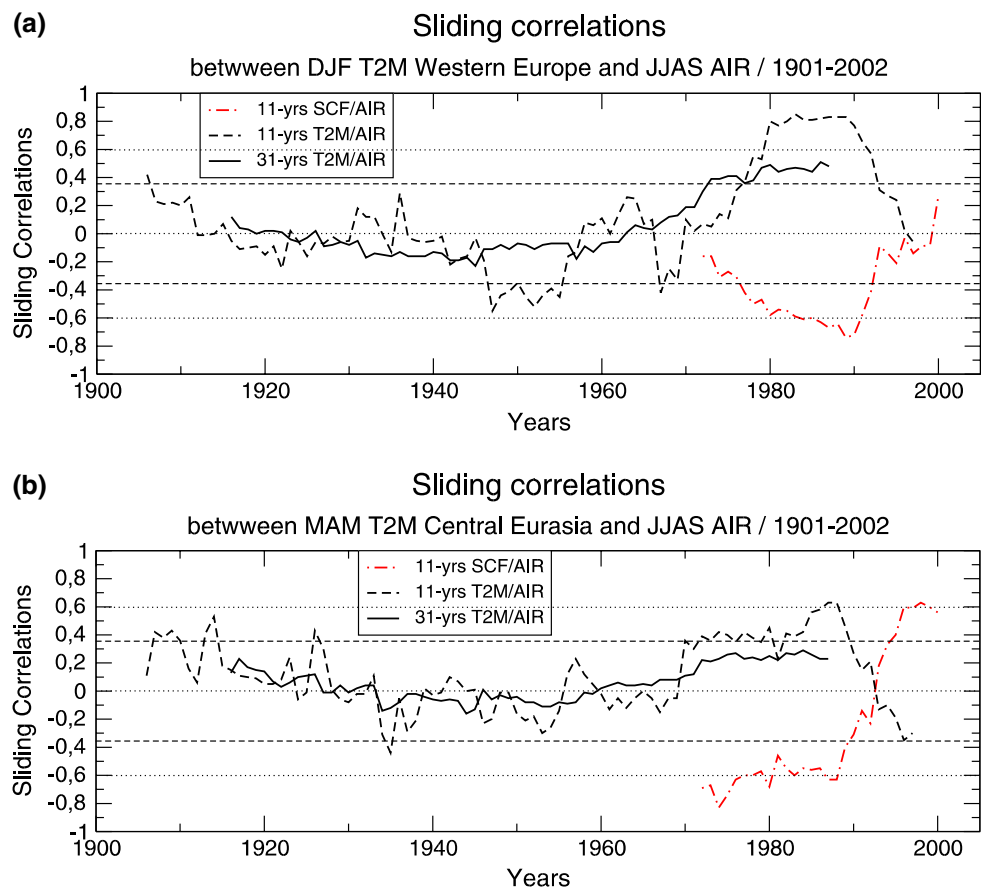

(a) Strong-Weak monsoons: snow cover DJF anomaly

5 years +   8 years -

-0.12 -0.08 -0.04   0   0.04   0.08   0.12

(b) Strong-Weak monsoons: snow cover MAM anomaly

5 years +   8 years -

-0.12 -0.08 -0.04   0   0.04   0.08   0.12

(c) Strong-Weak monsoons and neutral NAO (DJF): snow cover MAM anomaly

3 years +   5 years -

-0.12 -0.08 -0.04   0   0.04   0.08   0.12

Fig. 5 Sliding correlations between surface temperature (snow cover) and JJAS AIR for the period 1901–2002 (1967–2005): **a** in winter over western Europe; **b** in spring over central Eurasia. The *dashed* (*dotted*) *lines* correspond to the 95% confidence level for the 31-years (11-years) sliding correlations

the snow–monsoon relationship is not robust (i.e. statistically significant) and not necessarily consistent with the Blanford hypothesis.
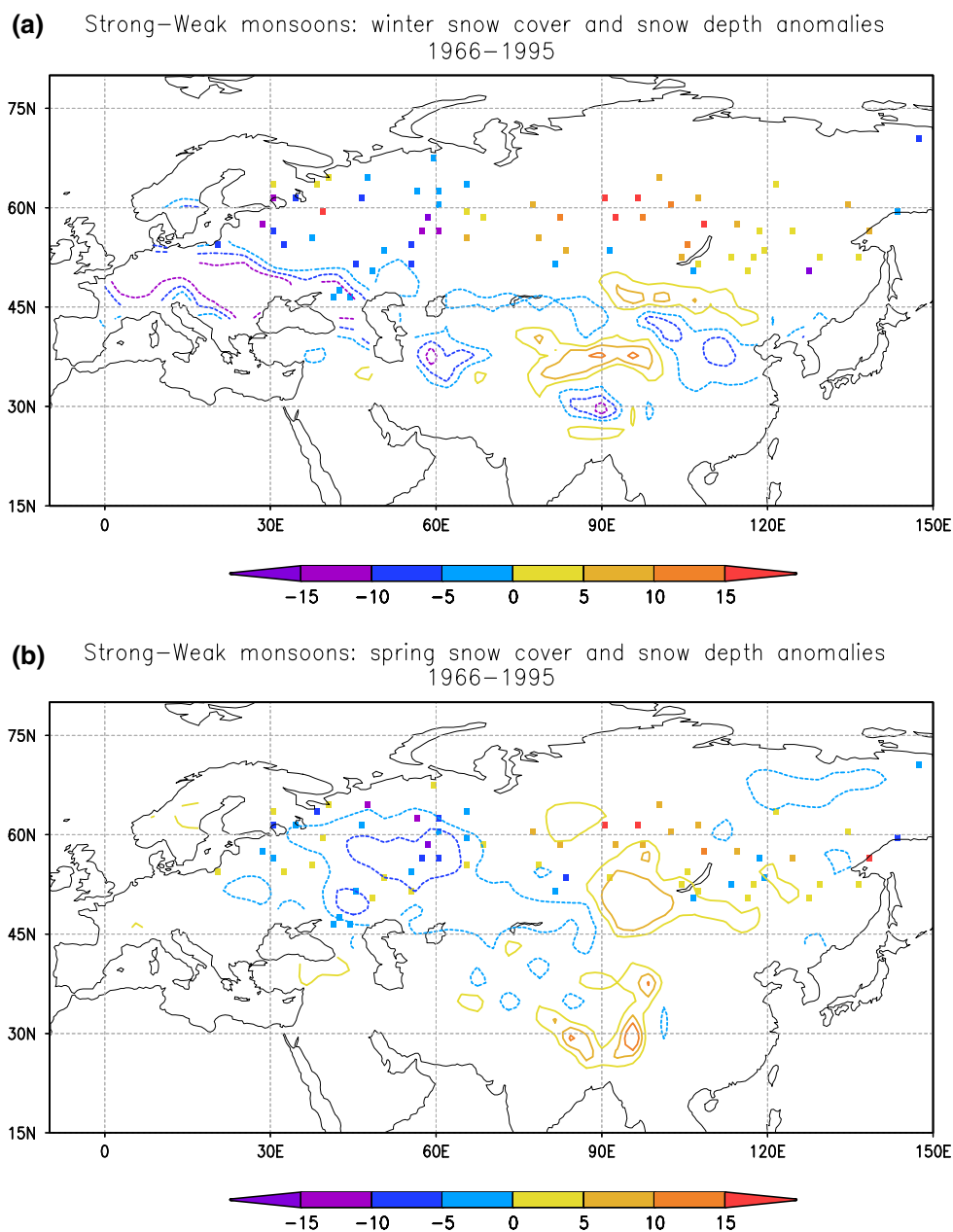
3.2 Stability of the snow–monsoon relationship

Anomalies of winter/spring snow cover fraction averaged over Eurasia [30–80N/20W–140E] and anomalies of summer AIR index are plotted on Figs. 2a and c, for the period 1967–2005. To evaluate the stability of the snow–monsoon link, sliding correlations have been calculated between snow cover and AIR using a 11-years sliding window for the period 1967–2005 (Figs. 2b, d). For winter and spring, we show sliding correlations for snow cover averaged over the entire Eurasian continent, and for the areas defined in Sect. 3.1 which show the strongest inverse relationship with the Indian monsoon rainfall. These areas are, respectively, western Europe (35–60N/10W–30E) in winter and Central Eurasia (40–65N/45–75E) in spring.

The correlations are not stationary for both seasons. In winter, negative sliding correlations are found during the first 10 years, in agreement with Hahn and Shukla (1976), as well as during the 1980s and 1990s, but are never really

significant. The correlations weaken after the mid-1990s and become positive at the beginning of the twenty-first century. The correlations over the whole 1967–2005 period are summarised in Table 2. In winter, the correlation fails to be significant for snow cover averaged over the entire Eurasian continent. In contrast, the confidence level is greater than 99% ($cc = -0.35$) when the winter snow cover is averaged over western Europe. In spring, the correlations are not significant at 90% confidence level and the sliding correlations show a relatively close behaviour as in winter.

Interestingly, the Blanford hypothesis has been verified before the 1990s, but has not been confirmed over recent decades. Such a multi-decadal modulation of the snow–monsoon relationship, which could be due solely to stochastic processes, is consistent with the "peaks" of scientific literature on this issue. For example, Dickson (1984) and Sankar-Rao et al. (1996) found strong negative correlations (-0.59 and -0.41) over the periods 1967–1980 and 1973–1990, respectively. Here, we show that snow cover averaged over Eurasia is not a robust predictor of the Indian monsoon rainfall, and that the only statistically significant link is found in the previous winter over western Europe.

(a) Strong−Weak monsoons: winter snow cover and snow depth anomalies 1966−1995

(b) Strong−Weak monsoons: spring snow cover and snow depth anomalies 1966−1995

Fig. 6 Composites of snow depth in centimeter (*tick marks*) and snow cover fraction (*contours*) for strong minus weak monsoons for the period 1966–1995: **a** winter snow cover, **b** spring snow cover. For snow cover the period is 1967–1995
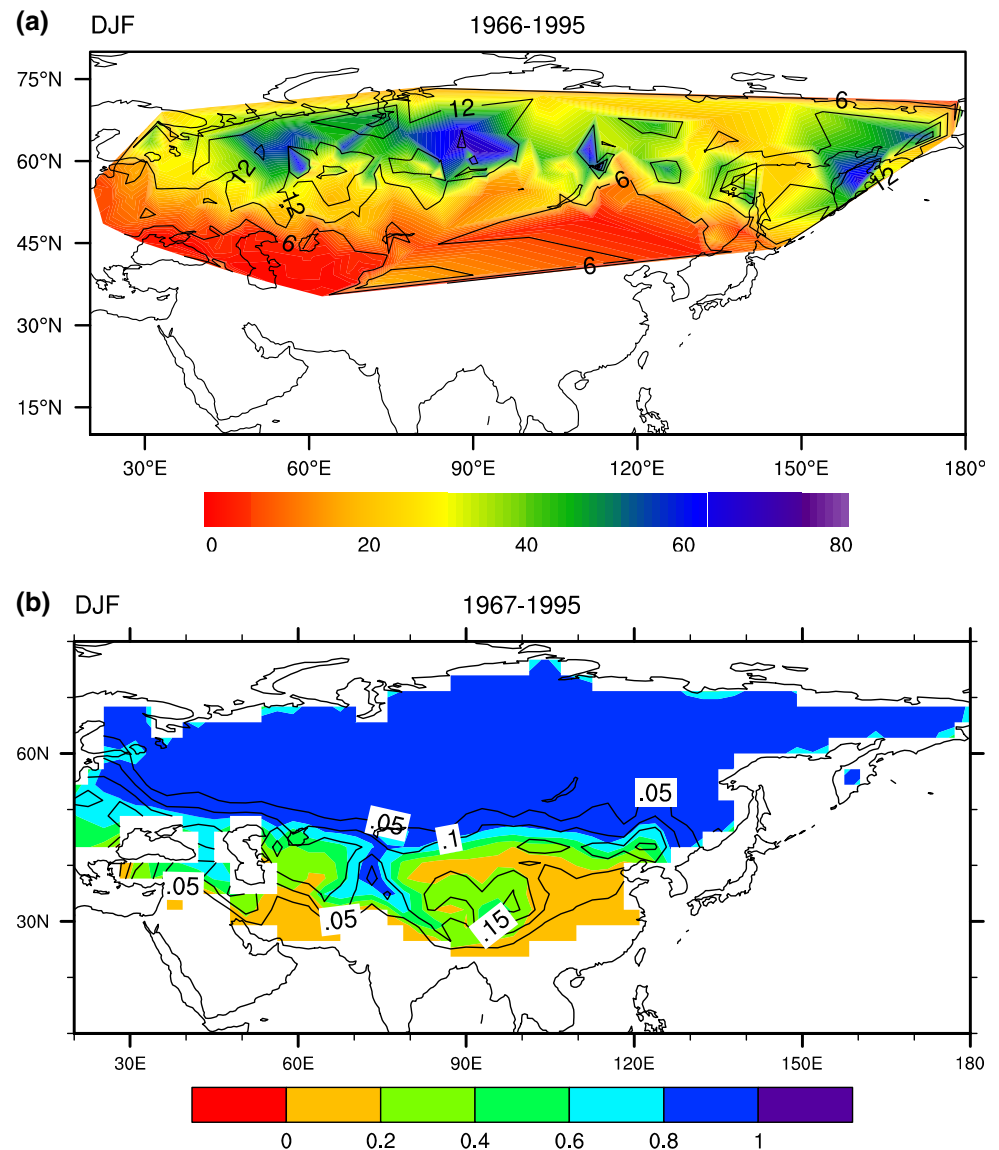
3.3 Stratified snow–ENSO–monsoon analysis

Several authors have discussed the Blanford hypothesis in term of an association between snow, ENSO and monsoon rainfall (Yang 1996; Fasullo 2004). They argued that the inverse snow–monsoon relationship is disrupted by El Niño/La Niña events. Yang (1996) suggested that deficient (excessive) Indian monsoon rainfall follows strong (weak) snow cover over Eurasia, but noted that this link is disrupted when an El Niño event occurs in winter and for weak La Niña years. They, however, emphasized the difficulty to assess the statistical significance of such effects due to their limited snow record (1972–1990), and noted the importance of replacing winter by spring snow cover.

Figure 3 shows the scatterplot between winter/spring snow cover anomalies averaged over Eurasia and the following JJAS AIR anomalies. The preceding DJF El Niño/La Niña years are indicated, they are defined based on anomalies in DJF Niño3 [SST 5S–5N/150–90W], whose standard deviation exceeding 0.9. This criterion was chosen to select a reasonable number of "ENSO" years. In keeping with Yang (1996), we cannot conclude about the reality of the Blanford hypothesis. In fact, only 16 (11) years among the 27 years without ENSO events in winter (spring) correspond to a negative snow–monsoon relationship. The maximum correlation between ENSO and the Indian summer monsoon being synchronous, the same analysis was conducted by focusing on the years without

Fig. 7 Climatological mean (*shaded*) and standard deviation (*contours*) for winter: **a** snow depth in cm, **b** snow cover fraction, for the period 1996–1995 (1967–1995 for snow cover)

ENSO signal in summer (JJAS). With winter (spring) snow cover, we only found 12 (9) years verifying the Blanford hypothesis (not shown), which is still not sufficient to conclude on the reality of the snow–monsoon link.

3.4 Composite analysis

The significant correlation found between monsoon rainfall and the winter snow cover over western Eurasia is confirmed by the snow cover composite for strong minus weak monsoon seasons (Fig. 4a). Statistically significant anomalies are found over Europe and support an inverse snow–monsoon relationship over this region. Figure 4b shows the same composite in spring. Snow cover shows negative (positive) anomalies in central Eurasia before a strong (weak) monsoon season. The signal is relatively noisy at the continental scale, but looks significant over Central Eurasia. Another region of significant anomalies appears over northern Siberia, in keeping with the results of Fasullo (2004), but it is probably not the signature of a direct snow forcing given the limited interannual variability of the springtime snow cover over this region.

Our results are consistent with those of Robock et al. (2003), though we have smaller areas of significant anomalies, which might be due to differences in the significance tests. They are difficult to interpret because of their weak significance, but in any case disagree with the Blanford hypothesis. To test the robustness of our results, we have conducted the same analysis after removing only 2 years for each composite, i.e. years when the DJF NAO index exceeds one standard deviation. In spring, the area of significant anomalies shifts toward eastern Eurasia (Fig. 4c).
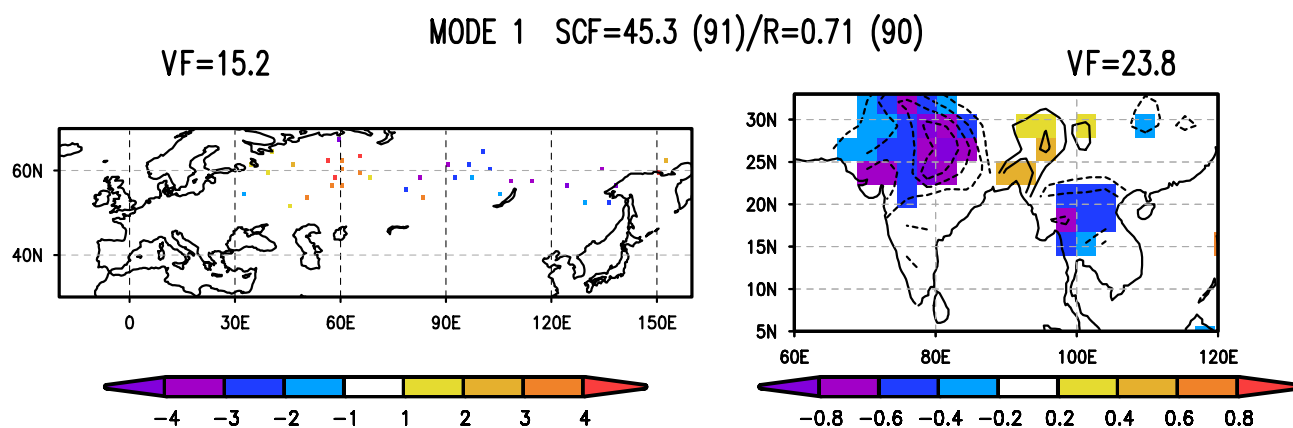
Fig. 8 Maximum covariance analysis between MAM snow depth in cm (left) and subsequent JJAS precipitation in mm/day (right) over the 1966–1995 period. First homogeneous vector is shown for snow depth and first heterogeneous vector for precipitation. The fraction of explained covariance (SCF) and the correlation between the two expansion coefficients are indicated, with the confidence level in parentheses

Table 3 Correlation coefficients between DJF and MAM seasonal snow depth anomalies over western Eurasia, central Eurasia and Eastern Eurasia and JJAS AIR for the periods 1936–1995 and 1966–1995

Domain	1966–1995 winter/spring	1936–1995 winter/spring
Western Eurasia [40–65N/25–75E]	−0.24/0.24	−0.22/−0.20
Central Eurasia [40–65N/45–75E]	−0.07/−0.19	−0.17/−0.20
Eastern Eurasia [40–65N/75–140E]	*0.66*/0.35	*0.33*/0.14

Values exceeding the 90%, 95% and 99% confidence levels are shown in italic, bold, bold and italic, respectively

The same result is obtained for winter composite (not shown) and suggests that a large part of the signal found in Fig. 4b is due to snow anomalies associated with strongly positive NAO. The NAO indeed exerts a strong influence on the western Eurasian snow cover (Robock et al. 2003), which could be an explanation for the link suggested here and in previous studies between the western/central Eurasian snow cover and the Indian monsoon. We do not conclude that the winter NAO exerts a strong influence on the Indian summer monsoon, but we argue that the snow–monsoon relationship is statistically not robust.

3.5 Temperature as a proxy for snow cover

The main obstacle for the analysis of the snow–monsoon relationship is the limited length of the satellite record. To get rid of this problem, we use the surface air temperature as a proxy for snow cover, just as Robock et al. (2003) used a DJF NAO index as a proxy. Surface air temperature and snow cover are indeed closely related over the regions highlighted in previous sections: the correlation for the period 1967–2002 is −0.72 in winter over western Europe [35–60N/10W–30E] and −0.79 in spring over central Eurasia [40–65N/45–75E]. These correlations are even stronger than those between our DJF NAO index and snow cover for the same period and regions (−0.57 and −0.19, respectively), so that surface air temperature is expected to be a better proxy for snow variability. The 11-year and 31-year sliding correlations between summer AIR and western (central) Eurasia winter (spring) surface air temperature are plotted in Fig. 5, as well as the corresponding 11-year sliding correlations with snow cover fraction. Recent decades show significant positive correlations in both winter and spring, in keeping with the inverse snow–monsoon relationship. However, this correlation is not stationary and fails to be significant during the major part of the twentieth century. The correlation with winter surface air temperature is particularly chaotic, with a period of negative correlations centred around 1950. For spring, the correlation is more stable but is not significant over the whole twentieth century.

Consequently, a persisting relationship between the twentieth century snow cover over western Eurasia in winter/spring and the Indian summer monsoon rainfall would imply that surface air temperature is not a robust or good enough proxy for the snow cover variability. Such a hypothesis is beyond the scope of the present study, but it would be interesting to analyse how the snow–temperature has evolved, both in the instrumental record and in the CMIP3 historical simulations.

3.6 A complementary analysis with snow depth

It is important to keep in mind that all results presented so far are based on satellite snow cover data. Consequently, we have no information on snow depth and the data mainly accounts for the radiative effect of snow. Yet, modelling studies have suggested that snow could also affect the
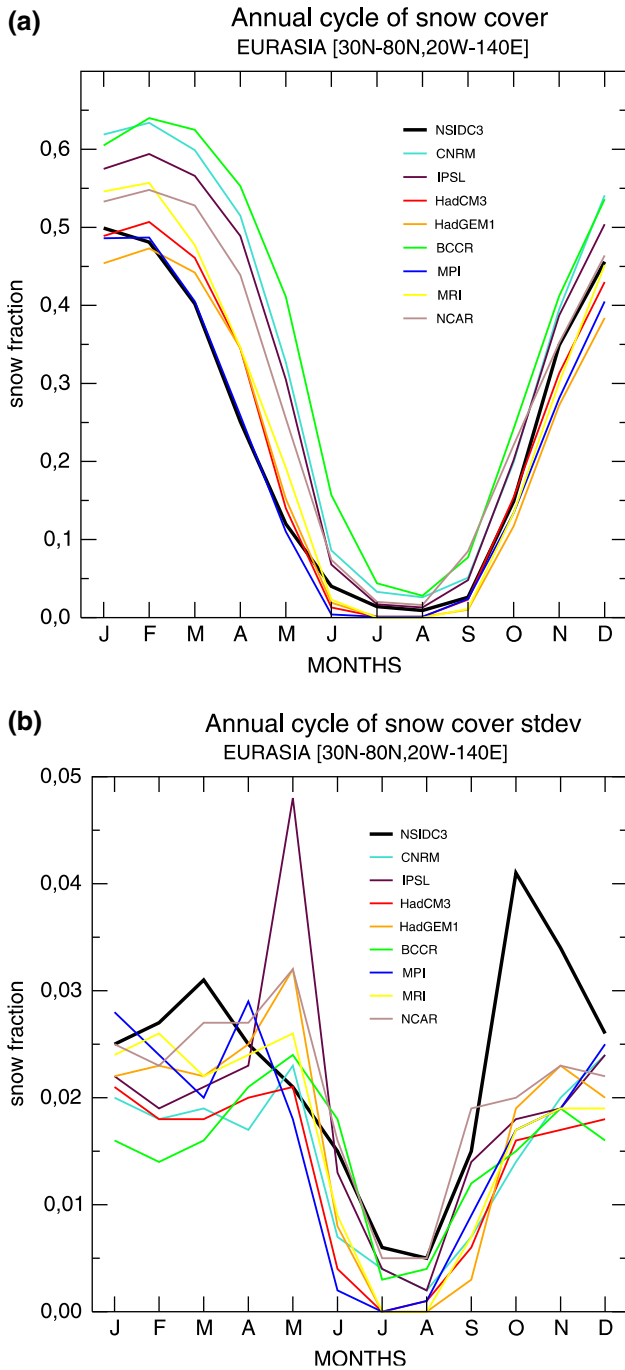
(a)

Annual cycle of snow cover
EURASIA [30N-80N,20W-140E]

(b)

Annual cycle of snow cover stdev
EURASIA [30N-80N,20W-140E]

Fig. 9 Climatological annual cycle of Eurasian snow cover: **a** monthly mean fraction, **b** monthly standard deviation

temperature of the Eurasian continent through the amount of energy necessary for snow-melting and subsequent soil moisture evaporation (Yasunari et al. 1991; Douville and Royer 1996). Difference between composites of snow depth and snow cover for strong-weak monsoons are shown in Fig. 6. Results obtained for snow depth are in good agreement with those for snow cover. In winter, snow

depth anomalies are more widespread than those found in snow cover. They are not confined to western Eurasia and already show a dipole pattern that is coherent with the spring composites. This result is in agreement with Ye and Bao (2001) and Dash et al. (2004) who have identified an opposite relationship of western/eastern Eurasia snow depth with the subsequent Indian summer monsoon rainfall. In winter, the snow cover fraction is close to 1 north of 50°N, so that its interannual variability in boreal regions is very weak compared to those of snow depth (Fig. 7). In spring, the snow line moves northward and the composites in term of snow cover and snow depth are therefore closer.

Figure 8 shows the MCA between snow depth over Eurasia in spring and precipitation over India in summer. For a statistically meaningful relationship, the MCA is computed over the period 1966–1995 for which there is very few missing data. Here again, the results support the conclusions obtained with snow cover. The first mode shows a dipole pattern of snow depth over Eurasia preceding an anomalous monsoon season over northern India. More (less) snow cover over western (eastern) Eurasia is followed by a weak monsoon. This mode is more robust than for the MCA computed with the snow cover data. The explained covariance fraction is larger, as well as the statistical significance in comparison with the MCA computed with snow cover. These results are consistent with the hypothesis that the strength of the monsoon is also influenced by snow hydrological effects rather than only radiative effects. However, they have to be considered with caution given the limited length of the snow depth dataset and its relative spatial scarcity. Table 3 summarizes correlation coefficients computed between western, eastern and entire Eurasia snow depth and AIR for two distinct periods, 1936–1995 and 1966–1995. Results confirm that the mean snow depth over western/eastern Eurasia exhibits an inverse/direct relationship with the following AIR.

Interestingly, snow depth over eastern Eurasia is better correlated with AIR than over western Eurasia. The greater correlation is obtained in winter, but this correlation is sustained through winter to spring where it is still significant at the 95% confidence level for the period 1966–1995. This link between the eastern Eurasian snow pack and the Indian monsoon is not found in term of snow cover because of the relatively weak interannual variability of snow cover in this region compared to the west of the continent. The physical mechanism behind this relationship is not intuitive and is in conflict with the usual Blanford hypothesis. Results suggest that the eastern Eurasian snow pack has not necessarily a direct impact on the Indian monsoon but shares a common sensitivity to large scale extratropical circulation anomalies that will be further described in a forthcoming study.
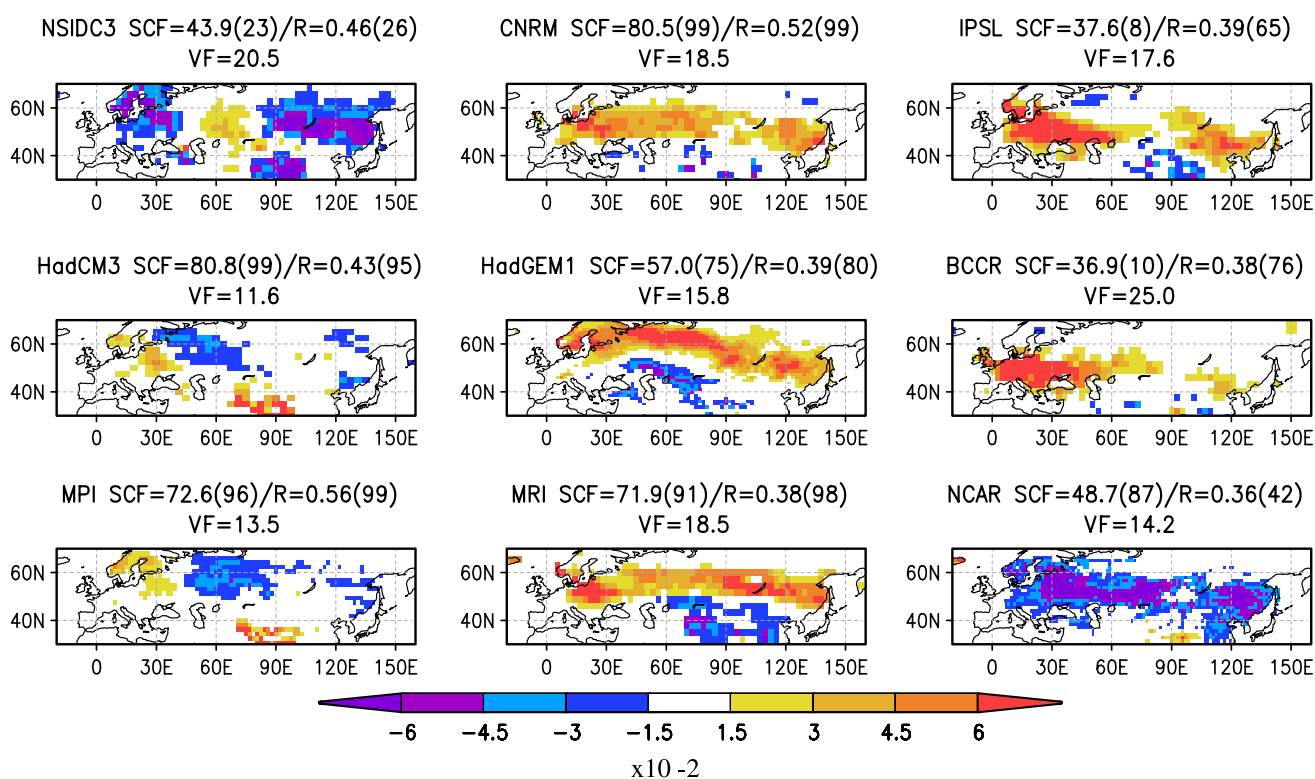
Fig. 10 First homogeneous vectors of snow cover fraction from a maximum covariance analysis between MAM snow cover and subsequent JJAS precipitation over the 1901–2000 period (1967– 2002 for observations). The fraction of explained covariance (SCF) and the correlation between the two expansion coefficients are indicated, with the confidence level in parentheses

4 Snow–monsoon relationship in the CMIP3 simulations

Another way to analyse the snow–monsoon relationship without the strong satellite constraint on the length of the timeseries is to use the monthly outputs of the historical CMIP3 simulations. The aim of this section is therefore to explore whether state-of-the-art coupled ocean-atmosphere models are likely to simulate the interannual variability of the Eurasian snow cover and its possible impact on the Indian summer monsoon. The focus is on snow cover rather than snow mass to compare with the most reliable observations and to avoid the spurious influence of mountainous areas where the lack of dynamical snow processes can lead to unrealistic snow accumulation in the models.

4.1 Snow annual cycle in the models

Snow cover is not a prognostic variable of the climate models, which use different diagnostic expressions to infer snow cover from snow mass. Moreover, for some models, the snow cover diagnostic is not provided on the CMIP3 database. In order to compare the models, it was therefore decided to derive a common monthly snow cover fraction, SC, from snow mass, WN, using the empirical formulation used in ARPEGE-Climate:

$$SC = WN/(WN + WN_{cr})$$

where WN_{cr} is a critical threshold of 10 kg/m^2. Such a simple expression is not aimed at capturing the complex relationship between snow mass and snow cover, but it provides a reasonable estimate that can be used to study the snow–monsoon relationship. While the model's climatology is obviously dependent on the value of WN_{cr}, the analysis of interannual variability is much less sensitive and the results of the present study are therefore fairly robust. Figure 9a shows the annual cycle of the Eurasian snow cover. Most models seem to overestimate the snow cover in spring, except the MPI model which shows a more realistic behaviour for this season. A possible explanation is that most models have a delayed snowmelt leading to an anomalous persistence of the snow pack in spring (Roesch 2006). However, all models are able to capture the main features of the snow annual cycle over Eurasia, with a strong increase in autumn and a rapid retreat in spring due to the snowmelt. As far as the annual cycle of interannual variability is concerned (Fig. 9b), the observed standard deviation peaks in March and mostly October, while most
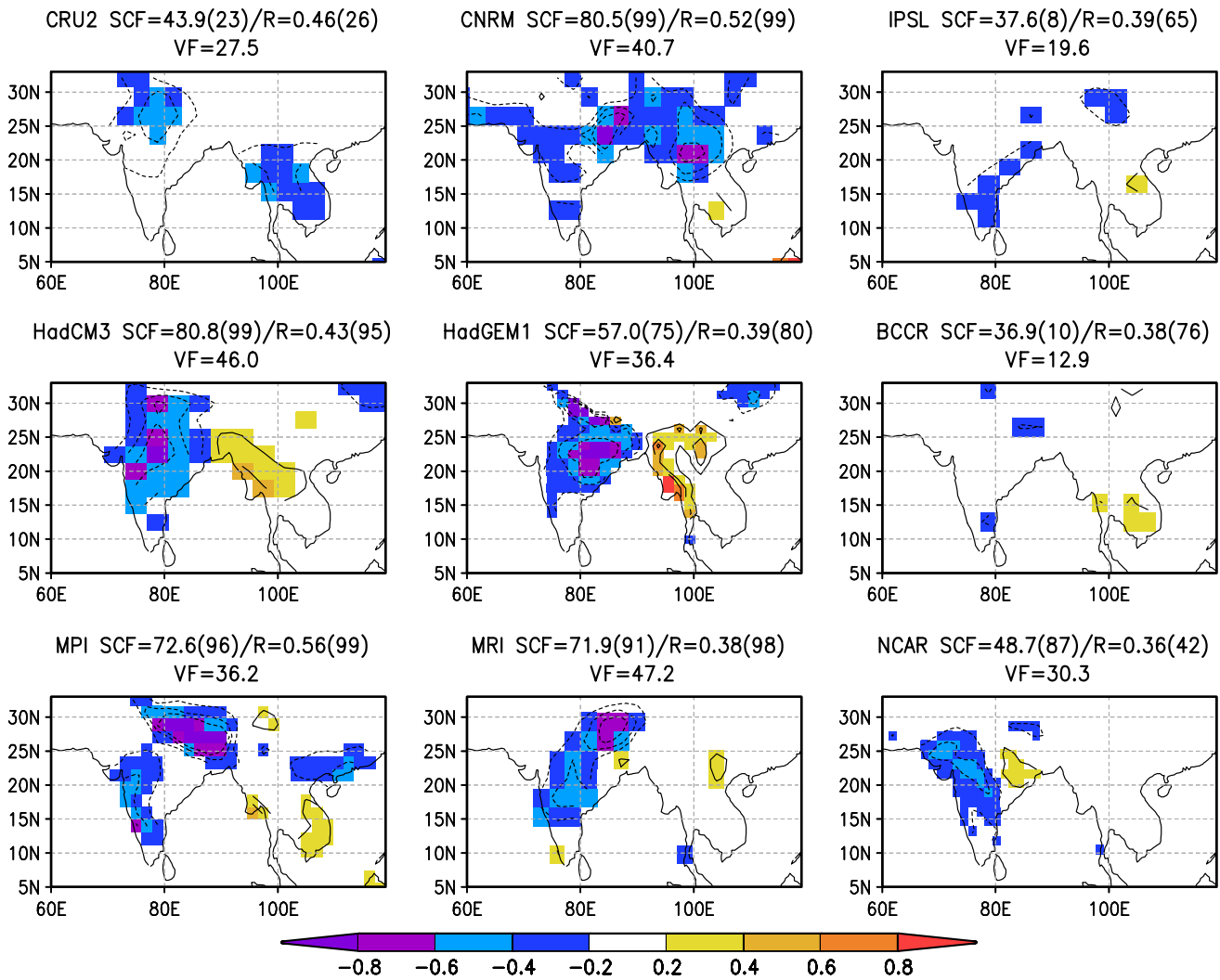
Fig. 11 First heterogeneous vectors of precipitation in mm/day from a maximum covariance analysis between MAM snow cover and subsequent JJAS precipitation over the 1901–2000 period (1967–2002 for observations). The fraction of explained covariance (SCF) and the correlation between the two expansion coefficients are indicated, with the confidence level in parentheses

Table 4 Correlation coefficients between: (1) expansion coefficients of first mode of MCA between MAM snow cover and JJAS P, (2) principal component of EOF from tropical SST DJF (winter ENSO)

Model	EC1 PN MAM	EC1 P JJAS
Observations (1967–2002)	0.06	0.20
CNRM	*0.49*	*0.79*
IPSL	0.10	0.04
HADCM3	*0.60*	*0.52*
HADGEM1	0.07	*0.26*
BCCR	0.14	*0.46*
MPI	*0.49*	*0.68*
MRI	**0.23**	−0.06
NCAR	0.10	0.06

Values exceeding the 90%, 95% and 99% confidence levels are shown in italic, bold, bold and italic, respectively

models show maximum values in May, in keeping with the delayed snowmelt.

4.2 Snow–monsoon relationship in the models

The link between the Eurasian snow cover and the Indian monsoon precipitation in the CMIP3 simulations is explored through a MCA between spring snow cover and summer precipitation over the same domains as for observations. Here again, snow cover and precipitation anomalies are filtered to keep only 60% of the explained variance for each field before the MCA calculation. Figures 10 and 11 show homogeneous vectors for snow and heterogeneous vectors for precipitation, respectively, and compare each of the nine models with the observations. The fractions of explained variance for snow and

precipitation range from 11.6 to 25.0% and from 12.9 to 47.2%, respectively. They are fairly sensitive to the prior filtering and tend to diminish when the criterion of residual variance is increased. Afterwards, we concentrate on models for which SCF and R significance reached the 90% confidence level, i.e. CNRM, MPI, HadCM3 and MRI.

- The model which shows the strongest snow–monsoon relationship is the CNRM model, where positive snow cover anomalies over the entire Eurasian continent precede a deficient South Asian monsoon. This result is consistent with the significant monsoon response found by Douville and Royer (1996) in a sensitivity experiment performed with a former and purely atmospheric version of the CNRM climate model.
- HadCM3 and MPI exhibit fairly robust and similar snow–monsoon links, but with a reverse snow pattern compared to the observations. An area of covariance also appears over the Tibetan Plateau which is in better agreement with the Blanford hypothesis.
- The first mode of MRI is a north-south dipole over the Eurasian continent, with more (less) snow on the northern (southern) part of Eurasia preceding a weak summer Indian monsoon.

In summary, none of the selected CMIP3 models is able to reproduce the observed patterns of covariability. Though some models show a robust relationship between the Eurasian or Himalayan snow cover and the Indian summer monsoon precipitation, it is difficult to identify a clear and consistent physical mechanism linking the interannual variability of snow and monsoon given the diversity of model behaviours.

4.3 Influence of ENSO on the snow–monsoon relationship in the models

In order to further explore the robustness of the snow–monsoon covariability simulated by CNRM, HadCM3, MPI and MRI, we now analyse the possible influence of ENSO on this relationship. Table 4 summarizes correlations between expansion coefficients of the two fields with the winter ENSO for all models. To obtain a robust ENSO index, we use the first EOF of a principal component analysis of DJF SST in the Tropics [32S–32N/0–360E]. Interestingly, three among the four models (CNRM, HadCM3 and MPI) exhibit a strong link between the two expansion coefficient timeseries, for snow and precipitation respectively, and the winter ENSO index. The ENSO–monsoon relationship is particularly exaggerated by CNRM and MPI with correlations close to 0.7 between the DJF ENSO index and the subsequent JJAS precipitation EC.

Figure 12 shows lead-lag correlations between the simulated JJAS precipitation over India [5–30N, 70–95E]
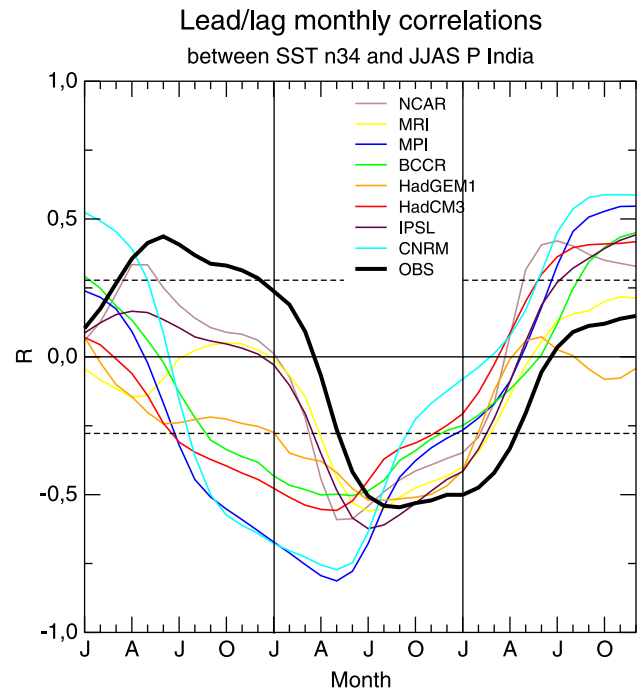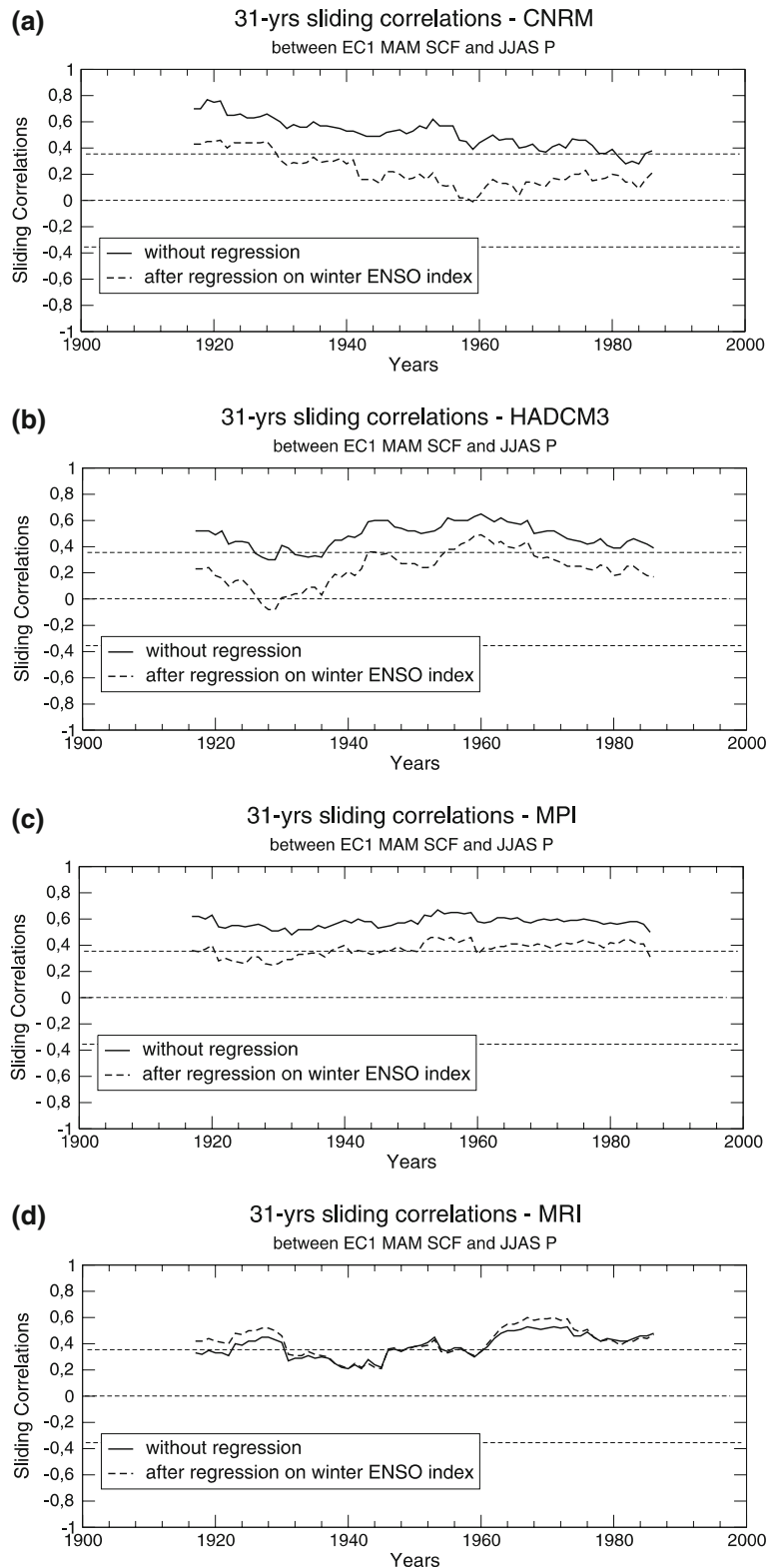

Fig. 12 Lead/lag correlation between monthly NINO3.4 SST index and summer precipitation averaged over India for observations and models. *Horizontal dashed lines* represent the 95% confidence level

and the monthly Niño3.4 [5S–5N, 170–120W] SSTs from the beginning of year −1 to the end of year +1. Observations show synchronous negative correlations with summer precipitation, which then persist until next winter. While this issue is still a matter of debate, the main interpretation is an ENSO influence on the monsoon that cannot be anticipated before the monsoon season because of the "spring barrier" of ENSO predictability, but is still apparent after the monsoon season given the locking of ENSO on the annual cycle and its usual peak in boreal winter.

Some models fail to reproduce the spring barrier and show significant negative correlations with the Niño3.4 SST after rather than before the ENSO events. This phenomenon was also found in the case of the West African monsoon by Joly et al. (2007) and was attributed to a common anomalous persistence of the ENSO events during spring. Here, CNRM, HadCM3 and MPI show the strongest negative correlations between winter ENSO and subsequent summer precipitation over India. This remark corroborates the results summarized in Table 4 and a spurious ENSO influence on global climate variability in these models.

Figure 13 illustrates the winter ENSO influence on the snow–monsoon link for the four models. Concerning CNRM, HadCM3 and MPI, while the sliding correlations between the two EC1 timeseries are relatively stable and are significant at the 95% confidence level during the

Fig. 13 Thirty-one years sliding correlation between spring snow cover expansion coefficients extracted from MCA calculation between Eurasian spring snow cover and Indian summer precipitation: **a** CNRM model, **b** HadCM3 model, **c** MPI model, **d** MRI model. Dashed curve represents result after regression of the timeseries on the first mode principal component of EOF from tropical winter SST. *Horizontal dashed lines* represent the 95% confidence level

whole twentieth century, they are much less significant when the ECs are regressed on the winter ENSO index by a simple linear regression. On the other hand, for MRI model the regression does not affect significantly the sliding correlations. Such results suggest that deficiencies in the ENSO simulation are partly responsible for the strong snow–monsoon relationship in three of the selected models. The MRI model is therefore the only one which

simulates a significant relationship between the Eurasian snow cover and the subsequent Indian summer monsoon independently of the phase of ENSO.

5 Summary and discussion

Understanding the interannual variability of the Indian summer monsoon and improving its seasonal predictability is a challenge for the climate modelling community as well as for more statisticians. While both ENSO and Eurasian snow influences have been documented, empirical and dynamical seasonal forecasting systems still show serious difficulties in predicting precipitation anomalies even at the sub-continental scale. Snow precursors are often considered in the empirical forecasting tools, but are still a matter of debate in both observational and numerical studies.

The first objective of the present study was to re-visit the observed snow–monsoon relationship, using an update of the NSIDC satellite data for snow cover from 1967 to 2006 as well as in situ snow depth data from 1936 to 1995. An east–west dipole pattern of snow cover anomalies associated with anomalous Indian monsoon precipitation was found over Eurasia in winter and spring accordingly with previous studies. Such a link is however neither stationary nor statistically significant over the whole 1967–2006 period, except for the winter snow cover over Europe which shows an inverse relationship with the subsequent Indian summer monsoon rainfall. The dipole pattern was also found in the snow depth record, but the strongest signal appears over eastern rather than western Eurasia and is not consistent with the Blanford hypothesis. Moreover, the use of surface air temperature as a proxy for snow cover over the whole twentieth century confirms the lack of robustness of the inverse snow–monsoon relationship.

The second objective of the study was to analyse a subset of historical CMIP3 simulations, in order to work with longer snow records and thereby to assess more robust though model-dependent statistical links. None of the models reproduce the east–west dipole pattern found in the observations. Some models do simulate a strong snow–monsoon relationship, but with different patterns and partly due to model deficiencies. On the one hand, most model climatologies show a delayed snowmelt in spring, which can favour the influence of snow cover anomalies on the summer monsoon. On the other hand, those models which show the strongest snow–monsoon relationship are also those which show an unrealistic impact of ENSO on both winter snow cover and summer monsoon.

In summary, the observed snow–monsoon relationship show a strong multi-decadal variability. The instrumental record is too short to explore the reasons for this, but such a modulation is probably compatible with a pure stochastic effect given the intrinsic variability of the Indian summer monsoon precipitation (Gershunov et al. 2000). Furthermore, state-of-the-art coupled ocean-atmosphere climate models still show serious deficiencies in both their extra-tropical and tropical variability, which make the simulated snow–monsoon relationship highly model-dependent and difficult to compare with observations. The snow–monsoon debate is therefore not over and will still deserve attention in a global warming climate with a decaying Eurasian snow cover.

References

Armstrong RL (2001) Historical Soviet daily snow depth version 2 (HSDSD). National Snow and Ice Data Center, Boulder, CO. CD-ROM

Armstrong RL, Brodzik MJ (2005) Northern Hemisphere EASE-Grid weekly snow cover and sea ice extent version 3. National Snow and Ice Data Center, Boulder, CO, USA. Digital media

Bamzai A, Shukla J (1999) Relation between Eurasian snow cover, snow depth and the Indian summer monsoon: an observational study. J Clim 12:3117–3132. doi:10.1175/1520-0442(1999)012<3117:RBESCS>2.0.CO;2

Barnett TP, Dumenil L, Schlese U, Roekler E, Latif M (1989) The effect of Eurasian snow cover on regional and global climate variations. J Atmos Sci 46:661–685. doi:10.1175/1520-0469(1989)046<0661:TEOESC>2.0.CO;2

Blanford HF (1884) On the connexion of Himalayan snowfall and seasons of drought in India. Proc R Soc Lond 37:3–22. doi:10.1098/rspl.1884.0003

Bretherton CS, Smith C, Wallace JM (1992) An intercomparison of methods for finding coupled patterns in climate data. J Climatol 5:541–560. doi:10.1175/1520-0442(1992)005<0541:AIOMFF>2.0.CO;2

Dash SK, Singh GP, Shekhar MS, Vernekar AD (2004) Response of the Indian summer monsoon circulation and rainfall to seasonal snow depth anomaly over Eurasia. Clim Dyn 24:1–10. doi:10.1007/s00382-004-0448-3

Dey B, Bhanu Kumar OSRU (1982) An apparent relationship between Eurasian snow cover and the advanced period of the Indian summer monsoon. J Appl Meteorol 21:1929–1932. doi:10.1175/1520-0450(1982)021<1929:AARBES>2.0.CO;2

Dey B, Kathuria SN, Kumar OB (1985) Himalayan summer snow cover and withdrawal of the Indian summer monsoon. J Appl Meteorol 24:865–868. doi:10.1175/1520-0450(1985)024<0865:HSSCAW>2.0.CO;2

Dickson RR (1984) Eurasian snow cover versus Indian monsoon rainfall—an extension of the Hahn-Shukla results. J Clim Appl Meteorol 23:171–173. doi:10.1175/1520-0450(1984)023<0171:ESCVIM>2.0.CO;2

Douville H, Royer JF (1996) Sensitivity of the Asian summer monsoon to an anomalous Eurasian snow cover within the Meteo-France GCM. Clim Dyn 12:449–466. doi:10.1007/BF02346818

Fasullo J (2004) A stratified diagnosis of the Indian Monsoon-Eurasian snow cover relationship. J Clim 17:1110–1122. doi:10.1175/1520-0442(2004)017<1110:ASDOTI>2.0.CO;2

Ferranti L, Molteni F (1999) Ensemble simulations of Eurasian snow-depth anomalies and their influence on the summer Asian monsoon. Q J R Meteorol Soc 125:2597–2610. doi:10.1002/qj.49712555913

Gershunov A, Schneider N, Barnett T (2000) Low-frequency modulation of the ENSO-Indian monsoon rainfall relationship: signal or noise? J Clim 14:2486–2492. doi:10.1175/1520-0442(2001)014<2486:LFMOTE>2.0.CO;2

Hahn DJ, Shukla J (1976) An apparent relation between Eurasian snow cover and Indian monsoon rainfall. J Atmos Sci 33:2461–2462. doi:10.1175/1520-0469(1976)033<2461:AARBES>2.0.CO;2

Helfrich SR, McNamara D, Ramsay BH, Baldwin T, Kasheta T (2007) Enhancements to, and forthcoming developments in the Interactive Multisensor Snow and Ice Mapping System (IMS). Hydrol Process 21:1576–1586. doi:10.1002/hyp.6720

Hurrell JW, Kushnir Y, Visbeck M, Ottersen G (2003) An overview of the North Atlantic oscillation. In: Hurrell JW, Kushnir Y, Ottersen G, Visbeck M (eds) The North Atlantic oscillation: climate significance and environmental impact. Geophysical Monograph Series, vol 134, pp 1–35

Joly M, Voldoire A, Douville H, Terray P, Royer JF (2007) African monsoon teleconnections with tropical SSTs in a set of IPCC4 coupled models. Clim Dyn 29:1–20. doi:10.1007/s00382-006-0215-8

Kripalani RH, Kulkarni A (1999) Climatology and variability of historical Soviet snow depth data: some new perspectives in snow—Indian monsoon teleconnection. Clim Dyn 15:475–489. doi:10.1007/s003820050294

Matsuyama H, Masuda K (1998) Seasonal/interannual variations of soil moisture in the former USSR and its relationship to Indian summer monsoon rainfall. J Clim 11:652–658. doi:10.1175/1520-0442(1998)011<0652:SIVOSM>2.0.CO;2

Nicholls N (2001) The insignificance of significance testing. Bull Am Meteorol Soc 82:981–986. doi:10.1175/1520-0477(2001)082<0981:CAATIO>2.3.CO;2

Parthasarathy B, Yang S (1995) Relationship between regional Indian summer monsoon rainfall and Eurasian snow cover. Adv Atmos Sci 12:143–150. doi:10.1007/BF02656828

Parthasarathy B, Munot A, Kothawale DR (1995) Monthly and seasonal rainfall series for all India homogeneous regions and meterological subdivisions. Research report RR-065: 113. Indian Institute of Tropical Meteorology, Pune, India

Rasmusson E, Carpenter T (1983) The relationship between eastern equatorial sea surface temperatures and rainfall over India and Sri Lanka. Mon Weather Rev 111:517–527. doi:10.1175/1520-0493(1983)111<0517:TRBEEP>2.0.CO;2

Robock A, Mu M, Vinnikov K, Robinson D (2003) Land surface conditions over Eurasia and Indian summer monsoon rainfall. J Geophys Res 108:4131. doi:10.1029/2002JD002286

Roesch A (2006) Evaluation of surface albedo and snow cover in AR4 coupled climate models. J Geophys Res 111:D15111. doi:10.1029/2005JD006473

Ropelewski CF, Robock A, Matson M (1984) Comments on "an apparent relationship between Eurasian snow cover and the advanced period of the Indian summer monsoon". J Clim Appl Meteorol 23:341–342. doi:10.1175/1520-0450(1984)023<0341:COARBE>2.0.CO;2

Sankar-Rao M, Lau MK, Yang S (1996) On the relationship between Eurasian snow cover and the Asian summer monsoon. Int J Climatol 16:605–616. doi:10.1002/(SICI)1097-0088(199606)16:6<605::AID-JOC41>3.0.CO;2-P

Shinoda M (2001) Climate memory of snow mass as soil moisture over central Eurasia. J Geophys Res 106:33393–33403. doi:10.1029/2001JD000525

Shukla J, Paolino D (1983) The Southern Oscillation and the long-range forecasting of monsoon rainfall over India. Mon Weather Rev 111:1830–1837. doi:10.1175/1520-0493(1983)111<1830:TSOALR>2.0.CO;2

Terray P, Delecluse P, Labattu S, Terray L (2003) Sea surface temperature associations with the late Indian summer monsoon. Clim Dyn 21:593–618. doi:10.1007/s00382-003-0354-0

Vernekar A, Zhou J, Shukla J (1995) The effect of Eurasian snow cover on the Indian monsoon. J Clim 8:248–266. doi:10.1175/1520-0442(1995)008<0248:TEOESC>2.0.CO;2

Von Storch H, Zwiers FW (1999) Statistical analysis in Climate Research. Cambridge University Press, London

Walker GT (1910) Correlations in seasonal variations of weather, II. Mem Indian Meteorol Dept 21:22–45

Walker GT (1924) Correlation in seasonal variations of weather. IV: a further study of world weather. Mem Indian Meteorol Dept 24:275–332

Wilks DS (1997) Resampling hypothesis tests for autocorrelated fields. J Clim 10:65–82. doi:10.1175/1520-0442(1997)010<0065:RHTFAF>2.0.CO;2

Yang S (1996) ENSO-Snow-Monsoon associations and seasonal-interannual predictions. Int J Climatol 16:125–134. doi:10.1002/(SICI)1097-0088(199602)16:2<125::AID-JOC999>3.0.CO;2-V

Yasunari T, Kitoh A, Tokioka T (1991) Local and remote responses to excessive snow mass over Eurasia appearing in the northern spring and summer climate—a study with the MRI GCM. J Meteorol Soc Jpn 69:473–487

Ye HC, Bao CH (2001) Lagged teleconnections between snow depth in northern Eurasia, rainfall in Southeast Asia and sea-surface temperatures over the tropical Pacific. Int J Climatol 21:1607–1621. doi:10.1002/joc.695